Towards Large-Domain Nonlinear System Identification of Multirotor Aircraft

Jeremy W. Hopwood* and Craig A. Woolsey†

Virginia Tech, Blacksburg, VA 24061

April 18, 2023

Abstract

High-fidelity, nonlinear flight dynamic models for multirotor aircraft important for the advancement of weather-tolerant advanced air mobility operations. The accuracy of these models directly affects the validity of safety and performance guarantees for guidance, navigation, and control algorithms. This paper presents a modeling and system identification approach for multirotor aerial vehicles. Lumped-parameter aerodynamics are obtained for an isolated rotor using blade-element and momentum theory, which are then incorporated into a six degree-of-freedom model for the multirotor aircraft. Critically, the obtained model is valid over a wide range of flight conditions, while also being identifiable from experimental data. Using a high-fidelity simulation constructed from wind tunnel data, the relative importance of model parameters is evaluated. This process then informs the final statistical estimation of model parameters.

1 Introduction

Developing technologies that guarantee safe and efficient advanced air mobility (AAM) operations are critical to pubic and governmental adoption of highly automated air transportation of people and goods in urban and suburban areas [1]. The importance of real-time weather prediction, wind observation, traffic management, and weather-tolerant operation increase as we elevate to higher maturity levels (UMLs) in NASA's AAM Vision Concept of Operations. These UMLs outline a need for higher weather tolerance and thus relaxed margins for flight safety [2]. As opposed to traditional aviation, safe aircraft operation in urban settings may rely on accurate in-situ wind estimation [3, 4], automation of air vehicle path planning and management [5], as well as new urban takeoff and landing technologies [6].

Achieving higher weather tolerance for AAM vehicles requires safety and performance guarantees across the levels of guidance, navigation, and control. The validity of these guarantees generally falls down to the fidelity of the flight dynamic model – i.e., how accurately a set of mathematical equations models the motion of the system. Flight dynamic models for aircraft are often represented as a low-dimensional system of ordinary differential equations to allow for direct use in control and estimation algorithms as well as efficient simulation and design optimization. Unlike the case for fixed-wing aircraft [7, 8, 9], there is no standard structure for compact, finite-dimensional models of multirotor flight. Typical approaches to multirotor modeling involve identifying linear state space models in the time domain or low order transfer functions in the frequency domain [10, 11, 12, 13, 14, 15]. Another approach is to identify a linear aerodynamic model for the nonlinear system [16]. Other common approaches include developing a simplified nonlinear aerodynamic model for a reduced number of degrees of freedom by assuming symmetry [17] and polynomial-based regressor determination using stepwise regression [18]. Multirotor modeling approaches often begin with the physical principles of a single rotor, superposing these effects to obtain a final model structure [19, 12]. However, a model that is valid within a larger domain, accurately capturing nonlinear dynamic and aerodynamic phenomena, may be required for stronger safety guarantees.

This paper describes the derivation, analysis, and identification of a multirotor flight dynamic model that is higher-fidelity than linear, small perturbation models, but easier to obtain and apply than models based on look-up tables of wind tunnel or computational/numerical data. Similar to [20], we begin with the forces and moments generated by a single rotor in forward flight derived using blade-element and momentum theories. This result is then incorporated into the forces and moments acting on the aircraft.

*Ph.D. Candidate, Kevin T. Crofton Department of Aerospace and Ocean Engineering, jeremyhopwood@vt.edu

†Professor, Kevin T. Crofton Department of Aerospace and Ocean Engineering, cwoolsey@vt.edu

The resulting nonlinear model is in a form amenable to identification from experimental data and control/estimator design. To evaluate the effectiveness of the postulated model structure, a simulation experiment was conducted using a high-fidelity multirotor aerodynamic model derived from wind tunnel data [21]. A statistically designed test matrix was developed to facilitate accurate identification of the unknown model parameters through a novel two-step regression approach.

2 Aircraft Rigid Body Dynamics

Consider a multirotor aircraft, modeled as a rigid body of mass m. Let unit vectors $\{\boldsymbol{i}_1, \boldsymbol{i}_2, \boldsymbol{i}_3\}$ define an earth-fixed North-East-Down (NED) orthonormal reference frame, $\mathcal{F}_\mathrm{I}$. As the notation $\mathcal{F}_\mathrm{I}$ suggests, we take this frame to be an inertial reference frame over the time and space scales of vehicle motion. Let the unit vectors $\{\boldsymbol{b}_1, \boldsymbol{b}_2, \boldsymbol{b}_3\}$ define the orthonormal body-fixed frame, $\mathcal{F}_\mathrm{B}$, centered at the aircraft center of gravity (CG) with $\boldsymbol{b}_1$ out the front of the aircraft, $\boldsymbol{b}_2$ out of the right-hand side, and $\boldsymbol{b}_3$ out of the bottom completing the right-hand rule. The position of the body frame with respect to the inertial frame is given by the vector $\boldsymbol{q} = [x\ y\ z]^\mathsf{T}$. The attitude of the aircraft is given by the rotation matrix, $\boldsymbol{R}_\mathrm{IB}$, that maps free vectors from $\mathcal{F}_\mathrm{B}$ to $\mathcal{F}_\mathrm{I}$. Let $\boldsymbol{v} = [u\ v\ w]^\mathsf{T}$ and $\boldsymbol{\omega} = [p\ q\ r]^\mathsf{T}$ be the translational and rotational velocity of the aircraft with respect to $\mathcal{F}_\mathrm{I}$ expressed in $\mathcal{F}_\mathrm{B}$, respectively. Let us represent the aerodynamic force and moment on the aircraft expressed in $\mathcal{F}_\mathrm{B}$ as $\boldsymbol{F}$ and $\boldsymbol{M}$, respectively. Let $\boldsymbol{I}$ be the moment of inertia matrix about the center of mass in $\mathcal{F}_\mathrm{B}$. Thus, the rigid body equations of motion are

$$\dot{\boldsymbol{q}} = \boldsymbol{R}_\mathrm{IB}\boldsymbol{v} \tag{1a}$$

$$\dot{\boldsymbol{R}}_\mathrm{IB} = \boldsymbol{R}_\mathrm{IB}[\boldsymbol{\omega}\times] \tag{1b}$$

$$\dot{\boldsymbol{v}} = \boldsymbol{v}\times\boldsymbol{\omega} + g\boldsymbol{R}_\mathrm{IB}^\mathsf{T}\boldsymbol{e}_3 + \frac{1}{m}\boldsymbol{F} \tag{1c}$$

$$\dot{\boldsymbol{\omega}} = \boldsymbol{I}^{-1}\left(\boldsymbol{I}\boldsymbol{\omega}\times\boldsymbol{\omega} + \boldsymbol{M}\right) \tag{1d}$$

where $[(\cdot)\times]$ is the skew-symmetric cross product equivalent matrix satisfying $[\boldsymbol{a}\times]\boldsymbol{b} = \boldsymbol{a}\times\boldsymbol{b}$ for 3-vectors $\boldsymbol{a}$ and $\boldsymbol{b}$. Here, the dependence of $\boldsymbol{F}$ and $\boldsymbol{M}$ on the aircraft and rotor states remains implicit, for now.

3 Rotor Aerodynamics

Consider a N_b-blade rotor of radius R rotating about its spin axis at the rate Ω $\frac{\mathrm{rad}}{\mathrm{s}}$ that is also steadily translating through still air with velocity $\boldsymbol{v}$ and airspeed $V = \|\boldsymbol{v}\|$. Let unit vectors $\{\boldsymbol{r}_1, \boldsymbol{r}_2, \boldsymbol{r}_3\}$ define a body-fixed orthonormal reference frame centered at the rotor hub with $\boldsymbol{r}_1$, $\boldsymbol{r}_2$, and $\boldsymbol{r}_3$ in the $-\boldsymbol{b}_1$, $+\boldsymbol{b}_2$, and $-\boldsymbol{b}_3$ directions, respectively, as shown in Figure 1. Note that the rotor frame is not defined such that the velocity vector is in the $\boldsymbol{r}_1$-$\boldsymbol{r}_3$ plane as typically done in rotor aerodynamics literature [22].

Since our goal is to develop a six degree-of-freedom model for a multirotor aircraft, we define *body axis advance ratios* μ_u, μ_v, μ_w and the *rotor-plane advance ratio* μ as

$$\mu_\star = \frac{\star}{\Omega R}, \quad \star \in \{u, v, w\} \tag{2a}$$

$$\mu = \frac{V_\mathrm{h}}{\Omega R} \tag{2b}$$

where $V_\mathrm{h} = \sqrt{u^2 + v^2}$ is the airspeed in the rotor plane. The *total inflow ratio*, λ, is

$$\lambda = \frac{\nu - w}{\Omega R} \tag{3}$$

where ν is the induced rotor inflow velocity (positive down), and w is the vertical velocity of the rotor expressed in the body frame (positive down).

Consider the thrust (T), hub force (H), side force (S), rolling moment ($\mathcal{R}$), pitching moment ($\mathcal{P}$), and torque ($\mathcal{Q}$) on a single rotor as shown in Figure 1. Recall, the free vector $\boldsymbol{v}$ is defined in the body frame, $\{\boldsymbol{b}_1, \boldsymbol{b}_2, \boldsymbol{b}_3\}$. As detailed in [22, Ch. 4], the rotor forces

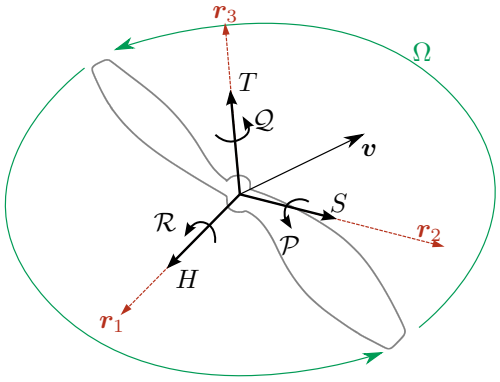

Figure 1: Rotor in forward flight

and moments can be obtained by integrating the force and moment acting on a differential element of the rotor blade. It is convenient to express these quantities as the non-dimensional coefficients,

$$C_T = \frac{T}{\rho\pi R^4\Omega^2} \quad C_\mathcal{R} = \frac{\mathcal{R}}{\rho\pi R^5\Omega^2}$$
$$C_H = \frac{H}{\rho\pi R^4\Omega^2} \quad C_\mathcal{P} = \frac{\mathcal{P}}{\rho\pi R^5\Omega^2} \tag{4}$$
$$C_S = \frac{S}{\rho\pi R^4\Omega^2} \quad C_\mathcal{Q} = \frac{\mathcal{Q}}{\rho\pi R^5\Omega^2}$$

Assumption 1. *For the purpose of rotor force and moment derivation, we assume the rotor blades*

a) *are rigid (no flapping);*

b) *do not stall;*

c) *have linear twist:* $\theta(\mathfrak{r}) = \theta_0 + \theta_{\text{tw}}\mathfrak{r}$*, where* $\mathfrak{r}$ *is the non-dimensional radial station along the blade measured from the hub.*

Denote the lift curve slope of a blade element as a and its mean drag coefficient as $\bar{c}_d$ (computed at $\mathfrak{r} = \sqrt{2}/2$). The rotor coefficients given as [22, Ch. 4]

$$C_H = C_\sigma \left[\frac{1}{2a}\bar{c}_d \mu_u + \left(\frac{\theta_0}{2} + \frac{\theta_{\text{tw}}}{4} \right) \lambda \mu_u \right] \tag{5a}$$

$$C_S = -C_\sigma \left[\frac{1}{2a}\bar{c}_d \mu_v + \left(\frac{\theta_0}{2} + \frac{\theta_{\text{tw}}}{4} \right) \lambda \mu_v \right] \tag{5b}$$

$$C_T = C_\sigma \left[\frac{\theta_0}{3}\left(1 + \frac{3}{2}\mu^2\right) + \frac{\theta_{\text{tw}}}{4}\left(1 + \mu^2\right) - \frac{\lambda}{2} \right] \tag{5c}$$

$$C_{\mathcal{R}} = C_\sigma \left[\frac{\theta_0}{3} + \frac{\theta_{\text{tw}}}{4} - \frac{\lambda}{4} \right] \mu_u \tag{5d}$$

$$C_{\mathcal{P}} = -C_\sigma \left[\frac{\theta_0}{3} + \frac{\theta_{\text{tw}}}{4} - \frac{\lambda}{4} \right] \mu_v \tag{5e}$$

$$C_{\mathcal{Q}} = C_\sigma \left[\frac{\bar{c}_d}{4a}\left(1 + \mu^2\right) + \left(\frac{\theta_0}{3} + \frac{\theta_{\text{tw}}}{4} - \frac{\lambda}{2} \right) \lambda \right] \tag{5f}$$

where $C_\sigma = \frac{N_\text{b}\bar{c}a}{2\pi R}$ for compactness. Note that the signs of the rotor coefficients come from the relationship between the body and rotor frames.

The inflow ratio, λ, is obtained from momentum theory. For a rotor in hover, the inflow velocity is $\nu_0 = \sqrt{\frac{mg}{2\rho A_\text{r}}}$, where A_r is the total rotor disk area of the aircraft, and ρ is the air density [23, Ch. 2]. However, we are interested in the more general forward flight condition where the inflow velocity is implicitly defined by $\nu = \nu_0^2/\sqrt{V_\text{h}^2 + (\nu - w)^2}$. To simplify the dependence on V_h and w, we choose to approximate this surface in the ν–V_h–w space by the plane

$$\nu \approx \nu_0 + C_{\nu_\mu} V_\text{h} + C_{\nu_w} w \tag{6}$$

Defining the *hover inflow ratio*, $\mu_0 = \frac{\nu_0}{\Omega R}$, the total inflow ratio, λ, can then be expanded and written as

$$\lambda = \mu_0 + C_{\nu_\mu}\mu + (C_{\nu_w} - 1)\mu_w \tag{7}$$

Next, the rotor coefficients in Eq. (5) are expanded using Eq. (7) to obtain the rotor force and moment coefficients

$$C_H = C_{H_{\mu_\text{b}}}\mu_u + C_{H_{\mu_\text{b},\mu_0}}\mu_u\mu_0 + C_{H_{\mu_\text{b},\mu}}\mu_u\mu - C_{H_{\mu_\text{b},\mu_w}}\mu_u\mu_w \tag{8a}$$

$$C_S = -C_{H_{\mu_\text{b}}}\mu_v - C_{H_{\mu_\text{b},\mu_0}}\mu_v\mu_0 - C_{H_{\mu_\text{b},\mu}}\mu_v\mu + C_{H_{\mu_\text{b},\mu_w}}\mu_v\mu_w \tag{8b}$$

$$C_T = C_{T_0} - C_{T_{\mu_0}}\mu_0 - C_{T_\mu}\mu + C_{T_{\mu^2}}\mu^2 + C_{T_{\mu_w}}\mu_w \tag{8c}$$

$$C_{\mathcal{R}} = C_{R_{\mu_\text{b}}}\mu_u - C_{R_{\mu_\text{b},\mu_0}}\mu_u\mu_0 - C_{R_{\mu_\text{b},\mu}}\mu_u\mu + C_{R_{\mu_\text{b},\mu_w}}\mu_u\mu_w \tag{8d}$$

$$C_{\mathcal{P}} = -C_{R_{\mu_\text{b}}}\mu_u + C_{R_{\mu_\text{b},\mu_0}}\mu_u\mu_0 + C_{R_{\mu_\text{b},\mu}}\mu_u\mu - C_{R_{\mu_\text{b},\mu_w}}\mu_u\mu_w \tag{8e}$$

$$C_{\mathcal{Q}} = C_{Q_0} + C_{Q_{\mu_0}}\mu_0 + C_{Q_\mu}\mu - C_{Q_{\mu_w}}\mu_w - C_{Q_{\mu_0^2}}\mu_0^2 - C_{Q_{\mu,\mu_0}}\mu\mu_0 + C_{Q_{\mu_0,\mu_w}}\mu_0\mu_w + C_{Q_{\mu^2}}\mu^2 + C_{Q_{\mu,\mu_w}}\mu\mu_w - C_{Q_{\mu_w^2}}\mu_w^2 \tag{8f}$$

where unknown constants have been lumped together to define a new set of dimensionless parameters. Because, the aim is to identify a dynamic model from experimental data, these new lumped parameters will appear in the final multirotor model. The rotor aerodynamic analysis presented here provides a physically motivated model structure, but specific coefficient values will be determined from data for the complete aircraft, not from computations of the expressions above.

4 Multirotor Forces and Moments

The rotor aerodynamic forces and moments described by Eq. (8) are not exact representations of the actual forces and moments applied to the airframe. Here, we consider a number of other factors that influence a given rotor's effect on vehicle motion.

4.1 Motor Dynamics

While there are many approaches to the electric propulsion of multirotor aircraft, we consider the common assumption as considered in [24, 12] that the system composed of the motor and electronic speed controller is well-described by a DC motor model. It is often assumed that the armature inductance is sufficiently small such that the electrical dynamics of the motor can be ignored. Thus, we are left with

$$J_z \frac{\mathrm{d}\Omega}{\mathrm{d}t} = -\mathcal{Q}_\text{m} + \mathcal{Q} \tag{9}$$

where J_z is the moment of inertia of the motor about the $\boldsymbol{r}_3$ axis, $\mathcal{Q}_\text{m}$ is the torque applied by the motor, and $\mathcal{Q}$ is the aerodynamic torque. Like in [25], we recognize that the motor dynamics influence the

rigid body in three dimensions. Consider the ith motor with position $\boldsymbol{r}_i = [x_i \;\; y_i \;\; z_i]^\mathsf{T}$ in the body frame. Let $\boldsymbol{\Omega}_i = [0 \;\; 0 \;\; \sigma_i \Omega_i]^\mathsf{T}$ be its angular velocity vector with respect to the body frame, expressed in the body frame, where $\sigma_i \in \{-1, +1\}$ represents the rotor rotation direction according to the right-hand rule. Then,

$$\boldsymbol{J}\dot{\boldsymbol{\Omega}}_i = \boldsymbol{J}\boldsymbol{\Omega}_i \times \boldsymbol{\omega} - \boldsymbol{M}_{\mathrm{m},i} + \boldsymbol{M}_{\mathrm{r},i} \tag{10}$$

where $\boldsymbol{J} = \mathbf{diag}(J_x, J_y, J_z)$ is the moment of inertia matrix of the motor/rotor rigid body, $\boldsymbol{M}_{\mathrm{m},i}$ is the moment applied to the airframe at the base of the motor (hence the minus sign), and

$$\boldsymbol{M}_{\mathrm{r},i} = \sigma_i \begin{bmatrix} -\mathcal{R}_i \\ \mathcal{P}_i \\ -\mathcal{Q}_i \end{bmatrix} \tag{11}$$

is the aerodynamic moment on the ith rotor expressed in the body frame. Here, the rotor aerodynamic moments are each evaluated at the rotor local velocity expressed in the body frame, $\boldsymbol{v}_i$. Note that Eq. (10) contains the implicit assumption that $\Omega_i \gg r$ for all $i \in \{1, \cdots, N_\mathrm{r}\}$, where r is the aircraft yaw rate. Assuming knowledge of $\dot{\boldsymbol{\Omega}}_i$, an expression for $\boldsymbol{M}_{\mathrm{m},i}$ in terms of motor parameters and electrical states is not needed. Instead, we rearrange and simplify Eq. (10) to obtain the moment applied to the airframe by a single rotor,

$$\boldsymbol{M}_{\mathrm{m},i} = \boldsymbol{M}_{\mathrm{r},i} - \sigma_i J_z \begin{bmatrix} q\Omega_i \\ -p\Omega_i \\ \dot{\Omega}_i \end{bmatrix} \tag{12}$$

Equation (12) shows the relationship between the rotor aerodynamic moments derived in Section 3 and the moment applied to the rigid body by a single rotor. The terms $J_z q \Omega_i$ and $J_z p \Omega_i$ are the gyroscopic effects of the motor, and $J_z \dot{\Omega}_i$ is net motor torque.

The transmission of rotor aerodynamic forces is much simpler than that of the moments. By the relationship between the rotor and body frames and using Eq. (4), the aerodynamic force of the ith rotor applied to the airframe at the base of the motor is

$$\boldsymbol{F}_{\mathrm{m},i} = \boldsymbol{F}_{\mathrm{r},i} = \begin{bmatrix} -H_i \\ S_i \\ -T_i \end{bmatrix} \tag{13}$$

4.2 Multirotor Aerodynamics

With an understanding of how forces and moments are transmitted to the airframe from Section 4.1, and the individual rotor forces and moments developed in Section 3, we can derive expressions for the total force and moment on a multirotor aircraft. Let the total force and moment applied to the airframe be $\boldsymbol{F} = [F_x \;\; F_y \;\; F_z]^\mathsf{T}$ and $\boldsymbol{M} = [M_x \;\; M_y \;\; M_z]^\mathsf{T}$, respectively. Consider a multirotor aircraft whose configuration is defined by the following assumptions.

Assumption 2.

a) *The number of rotors, $N_\mathrm{r} \geq 4$, is even.*

b) *Neighboring rotors spin in opposite directions.*

c) *The rotor configuration is symmetric about the $\boldsymbol{b}_1$ and $\boldsymbol{b}_2$ axes.*

d) *The rotors arms have equal length, ℓ, and are arranged with equal interior angles, $2\pi/N_\mathrm{r}$.*

e) *The rotors are uncanted (coplanar) and located at the same height, $h = -z_i$, above the CG.*

As an example, a quadrotor in an "X" configuration as pictured in Figure 2 satisfies Assumption 2.

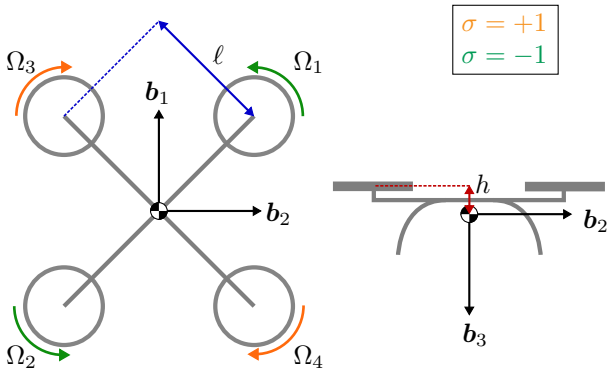

Figure 2: Quadrotor geometry

As it will be important for the final model, we define three classes of configurations that satisfy Assumption 2.

Definition 1. *A multirotor aircraft satisfying Assumption 2 is called a*

a) **quadrotor$_+$** *if $N_\mathrm{r} = 4$ and $(x_i, y_i) = (0, \ell)$ for some $i \in \{1, 2, 3, 4\}$;*

b) **quadrotor$_\times$** *if $N_\mathrm{r} = 4$ and $(x_i, y_i) = (\ell\frac{\sqrt{2}}{2}, \ell\frac{\sqrt{2}}{2})$ for some $i \in \{1, 2, 3, 4\}$;*

c) **multirotor$_{\geq 6}$** *if $N_\mathrm{r} \geq 6$.*

To this point, we have not mentioned airframe-specific (rotor-independent) forces and moments. Since the blade-element theory indicates there are rotor aerodynamic effects that do not depend on rotor speeds, we assume the following.

Assumption 3. *The airframe-specific aerodynamic forces and moments and rotor-airframe interactions effects can be lumped into the rotor aerodynamics.*

Thus, the body frame force, $\boldsymbol{F}$, is equal to the total rotor aerodynamic force, $\boldsymbol{F}_\mathrm{r} = [X_\mathrm{r} \;\; Y_\mathrm{r} \;\; Z_\mathrm{r}]^\mathsf{T}$:

$$\boldsymbol{F} = \boldsymbol{F}_\mathrm{r} = \sum_{i=1}^{N_\mathrm{r}} \boldsymbol{F}_{\mathrm{r},i} = \sum_{i=1}^{N_\mathrm{r}} \boldsymbol{F}_{\mathrm{m},i} \tag{14}$$

As shown in Section 4.1, however, $\boldsymbol{M}$ is not simply equal to the total rotor aerodynamic moment,

$$\boldsymbol{M}_\mathrm{r} = \sum_{i=1}^{N_\mathrm{r}} \left(\boldsymbol{M}_{\mathrm{r},i} + \boldsymbol{r}_i \times \boldsymbol{F}_{\mathrm{r},i}\right) =: \begin{bmatrix} \mathcal{L}_\mathrm{r} \\ \mathcal{M}_\mathrm{r} \\ \mathcal{N}_\mathrm{r} \end{bmatrix} \tag{15}$$

Instead, $\boldsymbol{M} = \sum_{i=1}^{N_\mathrm{r}} \left(\boldsymbol{M}_{\mathrm{m},i} + \boldsymbol{r}_i \times \boldsymbol{F}_{\mathrm{m},i}\right)$. Alternatively, the total applied moment, $\boldsymbol{M}$, can be written using the total aerodynamic moment in Eq. (15) as

$$\boldsymbol{M} = \boldsymbol{M}_\mathrm{r} - J_z \sum_{i=1}^{N_\mathrm{r}} \sigma_i \begin{bmatrix} q\Omega_i \\ -p\Omega_i \\ \dot{\Omega}_i \end{bmatrix} \tag{16}$$

Furthermore, we must determine for each rotor the contribution of vehicle angular velocity to the rotor aerodynamic forces and moments. These forces and moments are defined in the body frame whose origin does not coincide with the rotor hubs. Therefore, the velocity vector that defines the advance ratios in Eq. (2) should be the velocity vector at the rotor hub, which is equal to the sum of the body velocity vector, $\boldsymbol{v}$, and the velocity at the rotor's hub due to the vehicle's angular velocity, $\boldsymbol{\omega}$. Recalling from Assumption 2 that the rotors are not canted, i.e., the $\boldsymbol{r}_1$-$\boldsymbol{r}_2$ plane is parallel to the $\boldsymbol{b}_1$-$\boldsymbol{b}_2$ plane, the local velocity vector of the ith rotor in the body frame is

$$\boldsymbol{v}_i = \boldsymbol{v} + \boldsymbol{\omega} \times \boldsymbol{r}_i \tag{17}$$

Incorporating this correction yields a complicated model structure, however, that is difficult to identify from flight data. To obtain a more compact and identifiable form, we make the following assumption.

Assumption 4. *When computing the rotor forces and moments due to vehicle angular velocity, effects due to the vehicle yaw rate, r, and the vertical moment arm, h, can be neglected.*

Assumption 4 reflects the expectation that the primary contribution of the vehicle angular velocity to the rotor forces and moments is the resulting change in inflow velocity. Following Assumption 4, we approximate the local velocity of the ith rotor as

$$\boldsymbol{v}_i \approx \boldsymbol{v} + \begin{bmatrix} p \\ q \\ 0 \end{bmatrix} \times \begin{bmatrix} x_i \\ y_i \\ 0 \end{bmatrix} = \begin{bmatrix} u \\ v \\ w + py_i - qx_i \end{bmatrix} \tag{18}$$

While it is possible to identify a model with individual rotor speeds as inputs, this model would be less compact and less intuitive to analyze. Instead, we use the following *motor mixing* formula,

$$\underbrace{\begin{bmatrix} \delta^2 t \\ \delta^2 a \\ \delta^2 e \\ \delta^2 r \end{bmatrix}}_{\boldsymbol{\delta}^2} := \mathbf{M_{ix}} \underbrace{\begin{bmatrix} \Omega_1^2 \\ \Omega_2^2 \\ \vdots \\ \Omega_{N_\mathrm{r}}^2 \end{bmatrix}}_{\boldsymbol{\Omega}^2} \tag{19}$$

where $\mathbf{M_{ix}}$ is determined by aircraft geometry:

$$\mathbf{M_{ix}} = \begin{bmatrix} 1/N_\mathrm{r} & 1/N_\mathrm{r} & \cdots & 1/N_\mathrm{r} \\ -y_1 & -y_2 & \cdots & -y_{N_\mathrm{r}} \\ x_1 & x_2 & \cdots & x_{N_\mathrm{r}} \\ -\sigma_1 & -\sigma_2 & \cdots & -\sigma_{N_\mathrm{r}} \end{bmatrix} \tag{20}$$

Here, x_i and y_i are the $\boldsymbol{b}_1$ and $\boldsymbol{b}_2$ coordinates, respectively, of the ith rotor hub, and $\sigma_i \in \{-1, +1\}$ represents the rotor rotation direction according to the right-hand rule in the body frame. To capture first-order rotor speed terms, we also define

$$\underbrace{\begin{bmatrix} \delta t \\ \delta a \\ \delta e \\ \delta r \end{bmatrix}}_{\boldsymbol{\delta}} := \mathbf{M_{ix}} \underbrace{\begin{bmatrix} \Omega_1 \\ \Omega_2 \\ \vdots \\ \Omega_{N_\mathrm{r}} \end{bmatrix}}_{\boldsymbol{\Omega}} \tag{21}$$

In Eqs. (19) and (21), $\boldsymbol{\delta}^2$ and $\boldsymbol{\delta}$ are considered *virtual actuators*. Specifically, δa, δe, δr, and δt are referred to as virtual aileron, elevator, rudder, and thrust commands, respectively. Note, however, that $\boldsymbol{\delta}^2$ and $\boldsymbol{\delta}$ are not independently controlled.

Finally, the body frame forces and moments are obtained using Eqs. (14) and (16), where each $\boldsymbol{F}_{\mathrm{r},i}$ and $\boldsymbol{M}_{\mathrm{r},i}$ is evaluated at $\boldsymbol{v}_i$ as defined in Eq. (18) and rotor speeds are replaced using the virtual actuator definitions in Eqs. (19) and (21). As a result, the rigid-body force and moment components for a multirotor aircraft satisfying Assumption 2 are given in Eq. (22) (full derivation found in [26]). Note the configuration-dependent terms, $\Delta\nu_{(\cdot)}$, stem from the effect of angular velocity on the rotor inflow velocity.

This proposed model has several benefits when applied to control and estimation applications. Mainly, this model structure is valid over a large range of velocities. For flight in any direction, barring vortex ring state, there are very few approximations made. This model is also valid for large roll rate and pitch rate perturbations from translating flight because the local rotor velocity is incorporated directly. Furthermore, the use of virtual actuators not only generalizes

the model to any configuration satisfying Assumption 2, but also reveals an intuitive understanding of non-trivial effects such as $C_{H_{\mu_b}} R(u\delta a + v\delta e)$ in the yawing moment equation, M_z. This term captures the yawing moment due to differential drag under virtual aileron and elevator commands; it is similar to adverse/proverse yaw for fixed-wing aircraft.

$$F_x = \rho\pi R^2 N_\mathrm{r} u \left(-C_{H_{\mu_b}} R\delta t - C_{H_{\mu_b,\mu_0}} \nu_0 - C_{H_{\mu_b,\mu}} V_\mathrm{h} + C_{H_{\mu_b,\mu_w}} w\right) \tag{22a}$$

$$F_y = \rho\pi R^2 N_\mathrm{r} v \left(-C_{H_{\mu_b}} R\delta t - C_{H_{\mu_b,\mu_0}} \nu_0 - C_{H_{\mu_b,\mu}} V_\mathrm{h} + C_{H_{\mu_b,\mu_w}} w\right) \tag{22b}$$

$$F_z = \rho\pi R^2 \Big(- C_{T_0} R^2 N_\mathrm{r} \delta^2 t + C_{T_{\mu_0}} R N_\mathrm{r} \nu_0 \delta t + C_{T_\mu} R N_\mathrm{r} V_\mathrm{h} \delta t - C_{T_{\mu^2}} N_\mathrm{r} V_\mathrm{h}^2 - C_{T_{\mu_w}} R(N_\mathrm{r} w \delta t - \Delta\nu_z)\Big) \tag{22c}$$

$$\begin{aligned} M_x = \rho\pi R^2 \Big(& C_{R_{\mu_b}} R^2 u\delta r + C_{T_0} R^2 \delta^2 a - C_{T_{\mu_0}} R\nu_0 \delta a - C_{T_\mu} R V_\mathrm{h} \delta a + C_{T_{\mu_w}} R\Big(w\delta a - \Delta\nu_{\mathcal{L}}\Big) \\ & - C_{H_{\mu_b}} R N_\mathrm{r} h v \delta t - C_{H_{\mu_b,\mu_0}} N_\mathrm{r} h v \nu_0 - C_{H_{\mu_b,\mu}} N_\mathrm{r} h v V_\mathrm{h} + C_{H_{\mu_b,\mu_w}} N_\mathrm{r} h v w \Big) + J_z q \delta r \end{aligned} \tag{22d}$$

$$\begin{aligned} M_y = \rho\pi R^2 \Big(& C_{R_{\mu_b}} R^2 v\delta r + C_{T_0} R^2 \delta^2 e - C_{T_{\mu_0}} R\nu_0 \delta e - C_{T_\mu} R V_\mathrm{h} \delta e + C_{T_{\mu_w}} R\Big(w\delta e - \underset{\omega,\delta}{\Delta} w_{\mathcal{M}}\Big) \\ & + C_{H_{\mu_b}} R N_\mathrm{r} h u \delta t + C_{H_{\mu_b,\mu_0}} N_\mathrm{r} h u \nu_0 + C_{H_{\mu_b,\mu}} N_\mathrm{r} h u V_\mathrm{h} - C_{H_{\mu_b,\mu_w}} N_\mathrm{r} h u w \Big) - J_z p \delta r \end{aligned} \tag{22e}$$

$$\begin{aligned} M_z = \rho\pi R^2 \Big(& C_{Q_0} R^3 \delta^2 r + C_{Q_{\mu_0}} R^2 \nu_0 \delta r + C_{Q_\mu} R^2 V_\mathrm{h} \delta r - C_{Q_{\mu_w}} R^2 \Big(w\delta r - \Delta\nu_{\mathcal{N}}\Big) \\ & - C_{Q_{\mu_w^2}} R N_\mathrm{r} \ell^2 \Delta\nu_{\mathcal{N}}^2 - C_{H_{\mu_b}} R(u\delta a + v\delta e) - \frac{1}{2} C_{H_{\mu_b,\mu_w}} N_\mathrm{r} \ell^2 (up + vq) \Big) + J_z \dot{\delta} r \end{aligned} \tag{22f}$$

where $\Delta\nu_z = p\delta a + q\delta e$ and

$$\Delta\nu_{\mathcal{L}} = \begin{cases} \frac{1}{2}\ell^2 p(N_\mathrm{r}\delta t - \delta r) & \text{quadrotor}_+ \\ \frac{1}{2}\ell^2 (N_\mathrm{r} p\delta t + q\delta r) & \text{quadrotor}_\times \\ \frac{1}{2}\ell^2 p N_\mathrm{r}\delta t & \text{multirotor}_{\geq 6} \end{cases} \qquad \Delta\nu_{\mathcal{M}} = \begin{cases} \frac{1}{2}\ell^2 q(N_\mathrm{r}\delta t + \delta r) & \text{quadrotor}_+ \\ \frac{1}{2}\ell^2 (N_\mathrm{r} q\delta t + p\delta r) & \text{quadrotor}_\times \\ \frac{1}{2}\ell^2 q N_\mathrm{r}\delta t & \text{multirotor}_{\geq 6} \end{cases}$$

$$\Delta\nu_{\mathcal{N}} = \begin{cases} q\delta e - p\delta a & \text{quadrotor}_+ \\ -p\delta e - q\delta a & \text{quadrotor}_\times \\ 0 & \text{multirotor}_{\geq 6} \end{cases} \qquad \Delta\nu_{\mathcal{N}}^2 = \begin{cases} \frac{1}{2}(p^2 - q^2) & \text{quadrotor}_+ \\ pq & \text{quadrotor}_\times \\ 0 & \text{multirotor}_{\geq 6} \end{cases}$$

5 Quadrotor Simulation Experiment

A simulation study was conducted using a high-fidelity multirotor simulation [21] to investigate the utility of the proposed model structure. The rigid body forces and moments computed in the simulation are obtained from isolated rotor and airframe wind tunnel data. Thus, we are able to directly query the simulation's aerodynamics database at given vehicle state and control values in a similar manner to wind tunnel testing and computational aerodynamic prediction techniques. For this analysis, a simplified model assuming constant inflow velocity was used. This was done because the wind tunnel testing used to generate the simulation ignored non-trivial sideslip effects that would exemplify more complicated inflow velocity models. The effect of this simplification on Model (22) is the removal of terms that linearly depend on rotor-plane airspeed, V_h.

The test points were chosen using design of experiments and response surface methodology techniques to facilitate accurate identification of the terms included in the postulated model structure (see [4] for details). The ranges of explanatory variables considered in this study are listed in Table 1. The u and v body velocity components as well as the angular velocity bounds were chosen to be operationally representative for the vehicle size. The lower bound on vertical component w was chosen similarly, while the upper bound on w was chosen to be less than half the hover inflow velocity in order to avoid vortex ring state [27]. The bounds on the rotor speeds were chosen from the advance ratio limits

of the simulation wind tunnel lookup tables. Using the queried simulation data from the response surface experiment design, least squares parameter estimates were found for Model (22). A two step approach was used in which least squares regression was first performed independently for each force and moment equation to evaluate the relative importance of terms in the model. Next, a multivariate multiple regression (MMR) approach was used to obtain weighted least-squares parameter estimates for the complete model [28, Ch. 6].

Table 1: Explanatory variable ranges

Factor(s)	Units	Minimum	Maximum
u, v	ft/s	-60	+60
w	ft/s	-30	+5
p, q	deg/s	-720	+720
r	deg/s	-360	+360
$\Omega_1, \Omega_2, \Omega_3, \Omega_4$	rad/s	200	700

5.1 Regressor Ordering

First, the equation-error ordinary least-squares approach was used to estimate the model parameters for each force and moment equation independently (see [8, Ch. 5] and [28, Ch. 6]). The vector of N outputs for the ith force/moment equation is

$$\boldsymbol{y}_i = \boldsymbol{X}_i \boldsymbol{\theta}_i, \quad i \in \{1, \cdots, 6\} \tag{23}$$

where $\boldsymbol{\theta}_i \in \mathbb{R}^{p_i}$ is the vector of unknown parameters that appear in the ith equation and $\boldsymbol{X}_i \in \mathbb{R}^{N \times p_i}$ is the matrix of model regressors. Let $\boldsymbol{z}_i$ be the vector of "measured" outputs from the simulation data for the ith force/moment component. While the outputs at the test points are obtained without error, the underlying wind tunnel data contains random errors which are transferred into $\boldsymbol{z}_i$ in a nonlinear manner. We also recognize there is deterministic residual error between $\boldsymbol{y}_i$ and $\boldsymbol{z}_i$ due to unmodeled aerodynamics. For these reasons, the least-squares solution is not necessarily a minimum mean squared error or maximum likelihood estimate in the statistical sense.

Thus, the coefficient of determination, R^2, was used as the metric in a stepwise regression-like procedure to incrementally add all terms to the model in order of their contribution. Specifically, consider a model with p candidate regressors and let $\mathcal{C} = \{\boldsymbol{x}_1, \ldots, \boldsymbol{x}_p\}$, where each $\boldsymbol{x}_j$ represents a column of $\boldsymbol{X}_i$ in Eq. (23). We begin by considering a model with only one regressor and denote $\mathcal{I}$ (initially the empty set, $\varnothing$) as the ordered set of regressors already added to the model. Linear regression is performed for each of the candidate regressors in $\mathcal{C}$. The coefficients of determination are computed for each candidate regressor, and are denoted $R^2(\mathcal{I} \cup \{\boldsymbol{x}_i\})$. The regressor that yields the highest R^2 value, is then added to $\mathcal{I}$ and removed from $\mathcal{C}$. This process is repeated until all p terms are included in $\mathcal{I}$. This *forward selection ordering algorithm* (FSOA), is given in Algorithm 1.

Algorithm 1: FSOA

Input : $\mathcal{C} = \{\boldsymbol{x}_1, \ldots, \boldsymbol{x}_p\}$
Output: $\mathcal{I}$
$\mathcal{I} \leftarrow \varnothing$;
while $\mathcal{C} \neq \varnothing$ **do**
  $\boldsymbol{m} \leftarrow \underset{\boldsymbol{x} \in \mathcal{C}}{\operatorname{argmax}}\ R^2(\mathcal{I} \cup \{\boldsymbol{x}\})$;
  $\mathcal{I} \leftarrow \mathcal{I} \cup \{\boldsymbol{m}\}$;
  $\mathcal{C} \leftarrow \mathcal{C} \setminus \{\boldsymbol{m}\}$;
end

The FSOA results for F_x and F_z are given in Tables 2 and 3, respectively, as representative examples of the approach. The boldface values indicate the term that yields the highest R^2 value. For the models containing all regressors, the estimated model residual variances, $\hat{\sigma}_i^2 = \frac{1}{N-1}\sum_{k=1}^{N}(z_i(k) - \hat{y}_i(k))^2$, were also computed to inform the next step of regression.

Table 2: F_x FSOA results

	R^2 [%]		
Iter.	$C_{H_{\mu_b}}$	$C_{H_{\mu_b,\mu_0}}$	$C_{H_{\mu_b,\mu_w}}$
1	95.6	**98.0**	49.4
2	98.6	–	**98.7**
3	**99.3**	–	–
$\hat{\sigma}^2 = 3.70 \times 10^{-2}$			

Table 3: F_z FSOA results

	R^2 [%]			
Iter.	C_{T_0}	$C_{T_{\mu_0}}$	C_{z_μ}	$C_{T_{\mu_w}}$
1	**24.9**	18.9	−6.9	−93.3
2	–	25.9	24.9	**96.8**
3	–	96.8	**97.4**	–
4	–	**97.5**	–	–
$\hat{\sigma}^2 = 1.40$				

Using these results, we can relate each term back to the parameter definitions in Eq. (8) to obtain insight into the predominant physical effects of the model. In the F_x and F_y force components, the most influential model parameter is $C_{H_{\mu_b,\mu_0}}$, which is the lumped effect composed of drag due to induced inflow and the isolated airframe drag. In the Z_{r} force equation, the dominant term is $C_{T_0}\delta^2 t$, which comes

from the blade-element lift due to propeller speed. In the rolling and pitching moment equations, the most important term is $C_{T_0}\delta^2\{a, e\}$, which comes from the difference in lift due to the difference in rotor speeds. Finally, the primary effect in the yawing moment is $C_{Q_0}\delta^2 r$, which models the rotor profile drag due to the difference in rotor speeds.

5.2 Multivariate Multiple Regression

Recognizing that parameters appear across force and moment components, the estimates in Section 5.1 are not obtained using all possible data. For example, the parameter $C_{H_{\mu_b}}$ appears in all but the F_z equation, but is estimated five separate times. By using the results from the previous section, we can intelligently include data from all force/moment axes to simultaneously estimate these parameters which has three main benefits. First, the independent models for each axis may be overfit. This approach greatly reduces the total number of parameters to be identified. Second, all data are used to estimate the set of parameters. For example, $C_{H_{\mu_b}}$ can be estimated using five times as many measurements. Third, as will be detailed shortly, the residuals of the initial regression in Section 5.1 can justify a statistical interpretation of the final parameter estimates.

Considering all force and moment components as the output, we have the measurement model $\boldsymbol{y}(k) = \boldsymbol{H}(\boldsymbol{v}(k), \boldsymbol{\omega}(k), \boldsymbol{\Omega}(k))\boldsymbol{\theta}$, where $\boldsymbol{\theta} \in \mathbb{R}^{n_\theta}$ is the vector of proposed parameters and $\boldsymbol{H} : \mathbb{R}^3 \times \mathbb{R}^3 \times \mathbb{R}^{N_\mathrm{r}} \to \mathbb{R}^{6\times n_\theta}$ is the regressor function for the model. The "measured" output of this model is $\boldsymbol{z}(k) = \boldsymbol{y}(k) + \boldsymbol{w}(k)$, where each $\boldsymbol{w}(k)$ is assumed to be independently sampled from a Gaussian distribution. Let $\tilde{\boldsymbol{w}}(k) = \hat{\boldsymbol{y}}(k) - \boldsymbol{z}(k)$ where $\hat{\boldsymbol{y}}(k) = [\hat{y}_1(k) \ \cdots \ \hat{y}_6(k)]^\mathsf{T}$ was computed through the initial regression in Section 5.1. The covariance of $\boldsymbol{w}(k)$ is then approximated by $\boldsymbol{R} \approx \frac{1}{N-1}\sum_{j=1}^{N} \tilde{\boldsymbol{w}}(j)\tilde{\boldsymbol{w}}^\mathsf{T}(j)$. The diagonal elements of $\boldsymbol{R}$ for Model (22) are the estimated residual variances from the FSOA results. The validity of the Gaussian assumption is qualitatively evaluated by fitting a Gaussian probability density function to the histogram of residual data (Figure 3) and evaluating the linearity of the inverse cumulative distribution function (ICDF) with respect to the ordered model residuals. The model residuals appear to follow the shape of a normal distribution (shown as the red line in Figure 3), and the ordered residuals are largely linear with respect to the ICDF. Together, these results indicate that normality of the residuals is a reasonable assumption.

With the measurement model determined and random measurement errors characterized, statistical estimates of the model parameters were obtained using multivariate multiple regression [28, Ch. 6]. Let $\boldsymbol{\mathcal{Z}} = [\boldsymbol{z}(1) \ \cdots \ \boldsymbol{z}(N)]^\mathsf{T}$, and let $\boldsymbol{\mathcal{H}}$ and $\boldsymbol{\mathcal{W}}$ be defined similarly by vertically stacking the regressor functions and noise vectors. The stacked vector of model outputs is given by $\boldsymbol{\mathcal{Z}} = \boldsymbol{\mathcal{H}}\boldsymbol{\theta} + \boldsymbol{\mathcal{W}}$, and the stacked covariance matrix for $\boldsymbol{\mathcal{W}}$ is $\boldsymbol{\mathcal{R}} = \boldsymbol{R} \otimes \mathbb{I}_N$, where $\otimes$ is the Kronecker product and $\mathbb{I}_N$ is the $N \times N$ identity matrix. Then, the parameter estimates are given by the weighted least squares solution

$$\hat{\boldsymbol{\theta}} = (\boldsymbol{\mathcal{H}}^\mathsf{T}\boldsymbol{\mathcal{R}}^{-1}\boldsymbol{\mathcal{H}})^{-1}\boldsymbol{\mathcal{H}}^\mathsf{T}\boldsymbol{\mathcal{R}}^{-1}\boldsymbol{\mathcal{Z}} \tag{24}$$

Because each $\boldsymbol{w}(k)$ was assumed to be independently sampled from a zero-mean, Gaussian distribution, these parameter estimates are both minimum mean square error and maximum likelihood estimates. To evaluate model fit, both normalized root-mean square error (NRMSE) and Theil's inequality coefficient (TIC) were used [28, Ch. 11].

The overall MMR results for Model (22) are tabulated in Table 4. The R^2 and NRMSE values of the weighted least squared regression were 95.5% and 3.41%, respectively. The fit of the F_y model to the data is significantly worse than F_x. This is not the case, however when the airframe wind tunnel data is excluded from the study. This is perhaps an artifact of how the airframe side force was measured compared to the axial drag force.

The statistical significance of each of the identified parameters is evaluated using the t-statistic, $t_{0_j} = \hat{\theta}_j/\sigma(\hat{\theta}_j)$, where $\sigma(\hat{\theta}_j)$ is the estimated standard deviation of the $\hat{\theta}_j$. The null hypothesis,

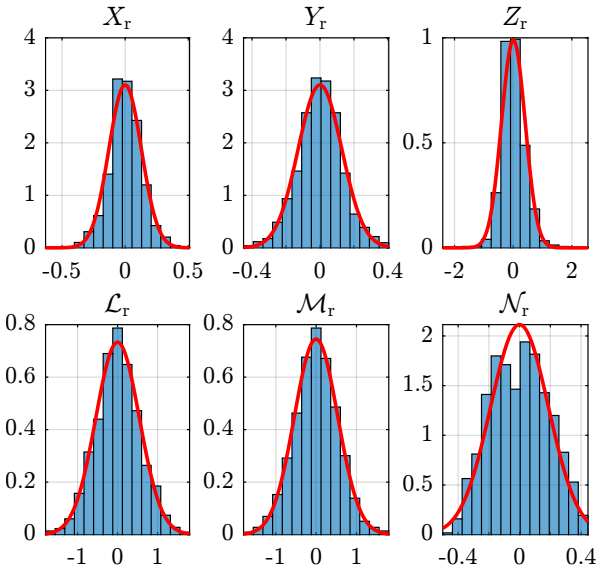

Figure 3: Probability density of residuals

Table 4: Model (22) MMR results

Component	NRMSE [%]	TIC
F_x	3.75	0.058
F_y	10.60	0.197
F_z	3.87	0.039
M_x	4.59	0.046
M_y	3.46	0.035
M_z	11.13	0.111

$H_0 : \hat{\theta}_j = 0$, is rejected with a significance level of α if $|t_{0_j}| > t(\alpha/2, N - n_\theta)$, and the alternate hypothesis, $H_1 : \hat{\theta}_j \neq 0$, is accepted. Here, $t(\alpha/2, N - n_\theta)$ is the sample of a one-tail t-distribution with confidence $\alpha/2$ and $N - n_\theta$ degrees of freedom. Alternatively, the P-value can be used to give the probability of the null hypothesis, H_0. In other words, it is the smallest significance level that results in the rejection of H_0. If $\mathrm{P}\{H_0\} < \alpha$, then H_0 is rejected and θ_j is statistically different from zero.

The parameter estimates ($\hat{\theta}$) computed using Eq. (24) are given in Table 5 along with their standard deviation (σ), t-statistic, and P-value (given to double precision). It can be seen that most parameter standard deviations are at least an order of magnitude less than their estimates. The notable exceptions are $C_{Q_{\mu_0}}$, $C_{Q_{\mu_w}}$, and $C_{Q_{\mu_w^2}}$. This is also seen in their t-statistics and P-values. While the underlying physics indicates the presence of these terms, their statistical significance is low for the simulation data. This result does not indicate these terms should be excluded, but rather their unique contribution to the yawing moment may be challenging to identify.

Table 5: Model (22) MMR parameter estimates

	$\hat{\theta} \times 10^2$	$\sigma \times 10^2$	$\lvert t_0 \rvert$	P-value
$C_{H_{\mu_b}}$	0.455	0.018	24.8	0.00
$C_{H_{\mu_b,\mu_0}}$	21.4	0.489	43.8	0.00
$C_{H_{\mu_b,\mu_w}}$	1.81	0.094	19.2	1.17×10^{-79}
C_{T_0}	1.54	0.028	55.2	0.00
$C_{T_{\mu_0}}$	3.11	0.752	4.1	3.67×10^{-5}
C_{z_μ}	−2.14	0.350	−6.1	1.14×10^{-9}
$C_{T_{\mu_w}}$	8.76	0.085	103.1	0.00
$C_{R_{\mu_b}}$	−1.12	0.111	−10.1	6.04×10^{-24}
C_{Q_0}	−0.136	0.039	−3.5	5.25×10^{-4}
$C_{Q_{\mu_0}}$	0.673	1.17	0.6	5.64×10^{-1}
$C_{Q_{\mu_w}}$	−0.031	0.118	−0.3	7.95×10^{-1}
$C_{Q_{\mu_w^2}}$	−5.28	16.0	−0.3	7.42×10^{-1}

6 Conclusions

Multirotor flight dynamic models for control and estimation have typically been limited to a small operating domain. This is, to some extent, due to the difficulty in connecting the well-established rotor aerodynamic theory to models that can be identified from experimental data. The results of this paper bridge the gap between rotor aerodynamic theory and flight dynamic modeling for control and estimation. By building up from blade-element and momentum theory, we are able to obtain a compact but accurate nonlinear flight dynamic model. Finally, a high-fidelity simulation study was used to evaluate regressor importance and estimate the proposed model parameters. This two-step approach can be readily extended to system identification of multirotor aircraft from flight data – a topic of future work.

Acknowledgments

The first author gratefully acknowledges the support of the Virginia Space Grant Consortium under the graduate research fellowship. The authors thank Benjamin Simmons and Jared Cooper for their ongoing collaboration and contribution to [26].

References

[1] "NASA Aeronautics Strategic Implementation Plan 2019 Update," tech. rep., National Aeronautics and Space Administration, 2019.

[2] M. Patterson, D. Isaacson, and N. Mendonca, "Intermediate State UAM Vision Concept of Operations (ConOps) Overview," Feb. 2021.

[3] C. Reiche, A. P. Cohen, and C. Fernando, "An Initial Assessment of the Potential Weather Barriers of Urban Air Mobility," *IEEE Transactions on Intelligent Transportation Systems*, vol. 22, pp. 6018–6027, Sept. 2021.

[4] J. W. Hopwood and C. A. Woolsey, "Passivity-Based Wind Estimation for Aircraft Maneuvering in Steady and Uniform Wind Fields," in *AIAA SciTech 2024 Forum*, AIAA, Jan. 2024.

[5] D. A. Karr, D. J. Wing, T. L. Barney, V. Sharma, T. J. Etherington, and J. L. Sturdy, "Initial Design Guidelines for Onboard Automation of Flight Path Management," in *AIAA AVIATION Forum*, July 2021.

[6] D. P. Thipphavong, R. Apaza, B. Barmore, V. Battiste, B. Burian, Q. Dao, M. Feary, S. Go, K. H. Goodrich, J. Homola, H. R. Idris, P. H. Kopardekar, J. B. Lachter, N. A. Neogi, H. K. Ng, R. M. Oseguera-Lohr, M. D. Patterson, and

S. A. Verma, "Urban Air Mobility Airspace Integration Concepts and Considerations," in *2018 Aviation Technology, Integration, and Operations Conference*, AIAA, June 2018.

[7] J. A. Grauer and E. A. Morelli, "Generic Global Aerodynamic Model for Aircraft," *Journal of Aircraft*, vol. 52, pp. 13–20, Jan. 2015.

[8] E. A. Morelli and V. Klein, *Aircraft System Identification: Theory and Practice*. Williamsburg, Virginia: Sunflyte Enterprises, second ed., 2016.

[9] B. M. Simmons, J. L. Gresham, and C. A. Woolsey, "Aero-Propulsive Modeling for Propeller Aircraft Using Flight Data," *Journal of Aircraft*, vol. 60, pp. 81–96, Jan. 2023.

[10] P. Niermeyer, T. Raffler, and F. Holzapfel, "Open-Loop Quadrotor Flight Dynamics Identification in Frequency Domain via Closed-Loop Flight Testing," in *AIAA Guidance, Navigation, and Control Conference*, p. 14, AIAA, Jan. 2015.

[11] M. I. Alabsi and T. D. Fields, "Real-Time Closed-Loop System Identification of a Quadcopter," *Journal of Aircraft*, vol. 56, pp. 324–335, Jan. 2019.

[12] M. A. Cunningham and J. E. Hubbard, "Open-Loop Linear Model Identification of a Multirotor Vehicle with Active Feedback Control," *Journal of Aircraft*, vol. 57, pp. 1044–1061, Nov. 2020.

[13] C. M. Ivler, E. S. Rowe, J. Martin, M. J. Lopez, and M. B. Tischler, "System Identification Guidance for Multirotor Aircraft: Dynamic Scaling and Test Techniques," *Journal of the American Helicopter Society*, 2021.

[14] R. Niemiec, C. Ivler, F. Gandhi, and F. Sanders, "Multirotor electric aerial vehicle model identification with flight data with corrections to physics-based models," *CEAS Aeronautical Journal*, vol. 13, pp. 575–596, July 2022.

[15] P. Wei, X. Lin, and Z. Kong, "System identification of wind effects on multirotor aircraft," *International Journal of Intelligent Robotics and Applications*, vol. 6, pp. 104–118, Mar. 2022.

[16] B. M. Simmons, "System Identification Approach for eVTOL Aircraft Demonstrated Using Simulated Flight Data," *Journal of Aircraft*, pp. 1–16, Feb. 2023.

[17] J. X. J. Bannwarth, Z. Jeremy Chen, K. A. Stol, B. A. MacDonald, and P. J. Richards, "Aerodynamic Force Modeling of Multirotor Unmanned Aerial Vehicles," *AIAA Journal*, vol. 57, pp. 1250–1259, Mar. 2019.

[18] S. Sun, C. C. de Visser, and Q. Chu, "Quadrotor Gray-Box Model Identification from High-Speed Flight Data," *Journal of Aircraft*, vol. 56, pp. 645–661, Mar. 2019.

[19] M. Bangura, *Aerodynamics and Control of Quadrotors*. PhD thesis, The Australian National University, Feb. 2017.

[20] G. Fay, "Derivation of the Aerodynamic Forces for the Mesicopter Simulation," (Stanford University), Stanford University, Feb. 2001.

[21] J. V. Foster and D. Hartman, "High-Fidelity Multi-Rotor Unmanned Aircraft System (UAS) Simulation Development for Trajectory Prediction Under Off-Nominal Flight Dynamics," in *17th AIAA Aviation Technology, Integration, and Operations Conference*, pp. 1–19, AIAA, June 2017.

[22] W. Johnson, *Helicopter Theory*. Princeton, N. J: Princeton Univ. Pr, 1980.

[23] J. G. Leishman, *Principles of Helicopter Aerodynamics*. Cambridge: Cambridge University Press, 2nd ed., 2006.

[24] W. Khan and M. Nahon, "Toward an Accurate Physics-Based UAV Thruster Model," *IEEE/ASME Transactions on Mechatronics*, vol. 18, pp. 1269–1279, Aug. 2013.

[25] E. J. J. Smeur, Q. Chu, and G. C. H. E. de Croon, "Adaptive Incremental Nonlinear Dynamic Inversion for Attitude Control of Micro Air Vehicles," *Journal of Guidance, Control, and Dynamics*, vol. 39, pp. 450–461, Mar. 2016.

[26] J. W. Hopwood, B. M. Simmons, C. A. Woolsey, and J. K. Cooper, "Development and Evaluation of Multirotor Flight Dynamic Models for Estimation and Control," in *AIAA SciTech 2024 Forum*, AIAA, Jan. 2024.

[27] J. Wolkovitch, "Analytical Prediction of Vortex-Ring Boundaries for Helicopters in Steep Descents," *Journal of the American Helicopter Society*, vol. 17, pp. 13–19, July 1972.

[28] R. V. Jategaonkar, *Flight Vehicle System Identification: A Time-Domain Methodology*. Progress in Astronautics and Aeronautics, Reston, Virginia: AIAA, Inc., second ed., 2015.